

Article

Lysine Dendrigrraft Nanocontainers. Influence of Topology on Their Size and Internal Structure

Boris Okrugin ¹, Maxim Ilyash ² , Denis Markelov ¹  and Igor Neelov ^{2,*} 

¹ Faculty of Physics, St. Petersburg State University, Ulyanovskaya Str.1, Petrodvorets, 198504 St. Petersburg, Russia; b.okrugin@spbu.ru (B.O.); d.markelov@spbu.ru (D.M.)

² St. Petersburg National University of Informational Technologies, Mechanics and Optics (ITMO University), Kronverksky pr.49, 197101 St. Petersburg, Russia; ilyashmu@gmail.com

* Correspondence: i.neelov@mail.ru; Tel.: +7-962-720-7977

Received: 1 July 2018; Accepted: 8 August 2018; Published: 13 August 2018



Abstract: Poly-L-lysine dendrigrrafts are promising systems for biomedical applications due to their biodegradability, biocompatibility, and similarity to dendrimers. There are many papers about the use of dendrigrrafts as nanocontainers for drug delivery. At the same time, the number of studies about their physical properties is limited, and computer simulations of dendrigrrafts are almost absent. This paper presents the results of a systematic molecular dynamics simulation study of third-generation lysine dendrigrrafts with different topologies. The size and internal structures of the dendrigrrafts were calculated. We discovered that the size of dendrigrrafts of the same molecular weight depends on their topology. The shape of all studied dendrigrrafts is close to spherical. Density profile of dendrigrrafts depends on their topology.

Keywords: poly-L-lysine; dendrigrrafts; molecular dynamics simulation

1. Introduction

Nowadays, there are many examples of the use of highly branched molecules—such as dendrimers, dendronized polymer brushes, dendrigrrafts, and hyperbranched polymers—for various industrial and biomedical applications. Dendrigrrafts are very similar to regular dendrimers, but they have a linear chain-like core instead of the usual point-like core in dendrimers. They also are slightly less regular than dendrimers. The main advantage of the dendrigrrafts is the low cost of their synthesis compared with the cost of dendrimers. One of the key features of the dendrimers is that the number of the terminal functional groups on the periphery increases exponentially with the generation number [1]. For this reason, dendrimers have many terminal groups available for functionalization, making them very popular for use in various nano-applications [2–6]. Biocompatible and biodegradable dendrimers and dendrigrrafts could be widely used in biomedical applications. Peptide dendrimers [7–14] and dendrigrrafts [15–18] consisting of amino acid residues are important examples of such dendrimers and dendrigrrafts. In particular, lysine dendrigrrafts of all generations have eight lysine residues in their core (see black circles in Figure 1). The poly-L-lysine PLL dendrigrrafts are biodegradable [15], have low cellular toxicity [16], and are nonimmunogenic [17]. For further information about the applications of dendrigrrafts, see references in paper [18].

Despite the popularity of PLL dendrimers and dendrigrrafts in applications, there are only a small number of experimental and theoretical papers devoted to the systematic study of physical properties and computer simulations of PLL dendrimers [19–23] and almost no papers on theory and computer simulations of PLL dendrigrrafts [18,24,25]. Our aim is to study the influence of the topology of the side chains on the size and internal structure of three third-generation dendrigrrafts by using a molecular dynamics simulation method.

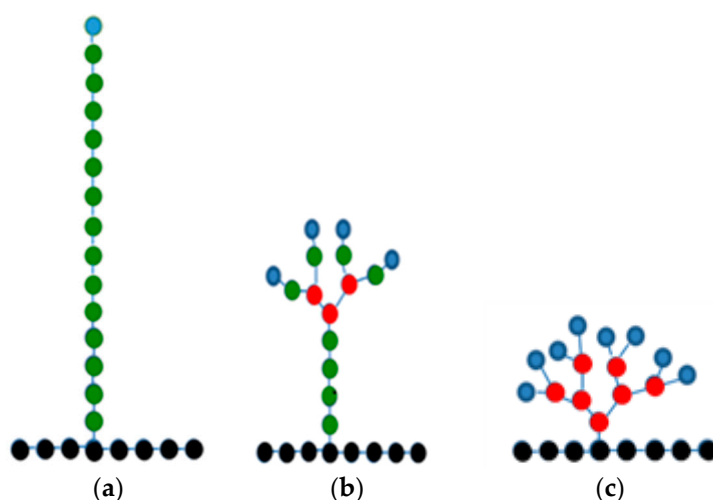


Figure 1. Three different lysine dendrigrafts: (a) dendrigraft 1; (b) dendrigraft 2; and (c) dendrigraft 3 with eight lysine residues in each main chain (core) marked by black points and 15 lysine residues (marked by green, red and blue points) in each of the eight side chains. Only one of the eight side chains is shown in Figure 1a–c for clarity: (a) dendrigraft 1, with 14 intermediate lysine residues (green), without branching lysine (red), and with one terminal lysine (blue) in each side chain; (b) dendrigraft 2, with eight intermediate lysines (green), three branching points (red), and four terminal lysine residues (blue) in each side chain; (c) dendrigraft 3, without intermediate lysine residues (green) and with seven branching points (red) and eight terminal lysine residues (blue) in each side chain.

2. Materials and Methods

We used a symmetrized model of third-generation lysine dendrigrafts in which all eight monomers of dendrigraft are the same. We constructed three monomers of different topologies. Each of the eight monomers of dendrigrafts contains one lysine residue in the main chain (marked in black in Figure 1a–c) and 15 lysine residues in the side chain (i.e., each of the eight dendrigraft monomers consists of 16 lysine residues). Each lysine residue in the side chain is either a branching point (marked in red in Figure 1), internal segment (green), or terminal segment (blue).

All three types of monomers have the same molecular weight M (see Table 1), but they have different topologies (number of branching points (marked by red in Figure 1a–c)) in side chains and number of terminal groups N_t (marked by blue) (see Figure 1 and Table 1). The side chain of the first monomer (of dendrigraft 1) is linear and thus does not have branching points. The side chain of the second monomer (of dendrigraft 2) has three branching points, and the side chain of the third monomer (of dendrigraft 3) has seven branching points. The branching points in Figure 1 (red) have no charge, each intermediate lysine residue (green) has one charge, and each terminal residue (blue) has two charges. After construction of the three different monomers and minimization of their energies, we connected them into a linear homopolymer chain consisting of eight monomers (using peptide bonds between circles marked by black in Figure 1). There are 16 lysine residues in each monomer of the third-generation dendrigraft (both in the main and side chain) and thus there are 128 lysine residues in the dendrigrafts as a whole. The total charge of each dendrigraft monomer will be equal to +16 and thus the total charge of all studied dendrigrafts consisting of 8 monomers will be equal to $+16 \times 8 = +128$.

The Gromacs-4.5.6 package [26] with AMBER99SB-ildn force field [27] was used in the simulations of all systems. Electrostatic interactions were calculated using the particle mesh Ewald (PME) method. The simulations of each dendrigraft consisted of the construction of an initial conformation of a system, minimization of its energy, equilibration of the system, and molecular dynamic (MD) simulation during 720 ns. Dendrigrafts were studied in a water solvent (TIP3P model) and Cl^- counterions were

added for compensation of dendrigraft charge. All calculations were performed at a temperature of 300 K and a pressure of 1 atm.

Table 1. Parameters of the simulated dendrigrafts: M is the molecular weight and N_t is the number of terminal groups.

Type	M (g/mol)	N_t
Dendrigraft 1	2947	8
Dendrigraft 2	2947	32
Dendrigraft 3	2947	64

Three systems consisting of dendrigrafts with the same molecular weight, but with different side chain topology (and, as a result, with different side chain contour lengths and charge distributions), were constructed. To avoid interatomic overlap, additional energy minimization was performed for whole systems. The initial 600 ns were used in MD simulations for equilibration of the systems and the last 120 ns were used as productive runs for calculating the average values and distribution functions of different values (size, end-to-end distance, radial density, and charge distributions).

3. Results

3.1. Large-Scale Properties

The size of dendrigrafts can be calculated by instant mean-square gyration radius

$$R_g^2 = \frac{1}{M} \sum_i (m_i r_i^2), \quad (1)$$

where r_i is the distance between the i -th atom and center of mass (COM) of the dendrigraft, and m_i and M are the molecular mass of the i -th atom and all atoms of dendrigraft correspondingly. Summations were taken over all atoms of the dendrigraft. Time dependences of this value for all dendrigrafts are presented in Figure 2a. The averaging along the trajectory (during the last 120 ns of simulation) gives the mean square value of the R_g . For dendrigraft 1 $R_g = 3.42$ nm, for dendrigraft 2 $R_g = 2.64$ nm, and for dendrigraft 3 $R_g = 2.09$ nm. Thus, the increase of the branching degree from dendrigraft 1 to dendrigraft 3 leads to smaller dendrigraft size due to the decrease of the contour length of the side chains (see Figure 1). We can compare values of R_g obtained from our simulation with R_g calculated from experimental hydrodynamics radius R_h [28,29] using theoretical connection of R_g and R_h for undrained spherical molecules:

$$\frac{R_g}{R_h} = \sqrt{\frac{3}{5}} \quad (2)$$

The values of R_g calculated from MD simulations of dendrigraft 2 and dendrigraft 3 (2.64 nm and 2.09 nm, respectively) belong to the interval of values $R_g = 1.65$ – 2.65 nm ($R_h = 2.14$ – 3.43 nm) obtained by different experimental methods in [28,29], while our value of R_g for dendrigraft 1 is essentially higher than for the experimental ones.

The distribution function of the gyration radius is presented in the Figure 2b. One can see that distribution becomes increasingly narrower for dendrigrafts with higher numbers of branching points.

Another parameter that characterizes the dendrigraft is the end-to-end distance of the side chain, or the distance between the C_α atoms of the lysine residue in the main chain and the corresponding terminal NH_3^+ group (blue circles in Figure 1) of each of the eight side chains. The distribution function of these values is presented in Figure 3. The result is quite predictable because increasing the number of branching points from dendrigraft 1 to dendrigraft 3 leads to a decrease in the contour length of the side chains.

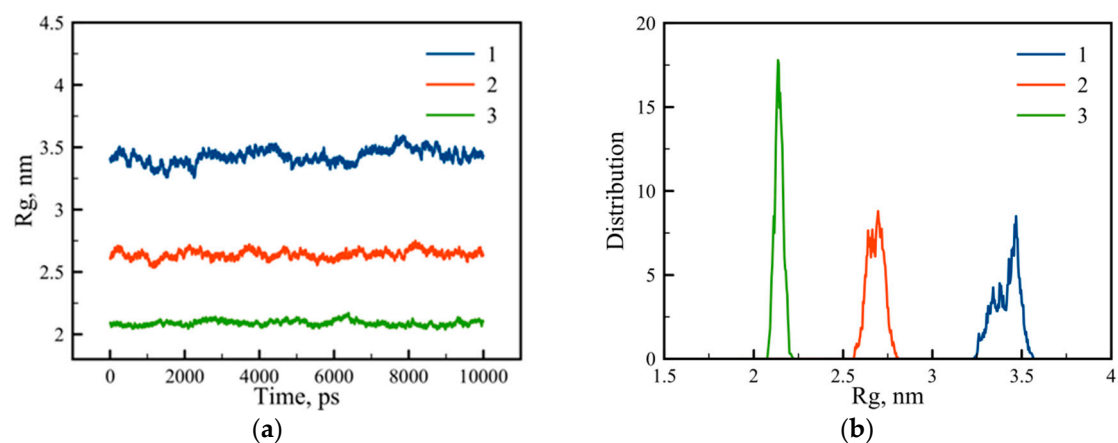


Figure 2. (a) The variation of the gyration radius R_g with time t in picoseconds and (b) the distribution function for dendrigrafts 1, 2, and 3.

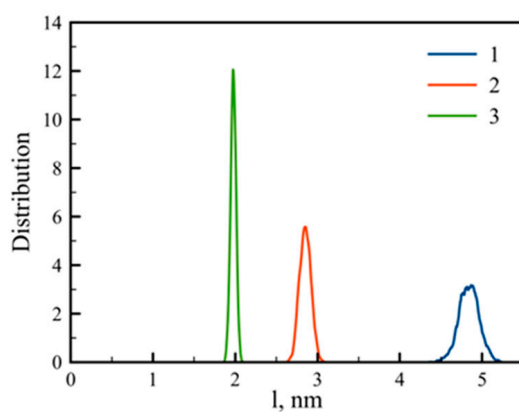


Figure 3. Distribution of side chain end-to-end distance (distance between the C_α atom of the main chain and terminal NH_3^+ group of the corresponding side chain) for dendrigrafts 1, 2, and 3.

Figure 4 shows snapshots of dendrigrafts simulated in this paper. It is easy to see that, similar to dendrimers [30–32], all studied dendrigrafts have a close to spherical shape despite their linear core. Due to this reason, we could calculate radial distribution of internal characteristics of these molecules, including the radial density and charge distributions around the center of mass of the dendrigrafts.

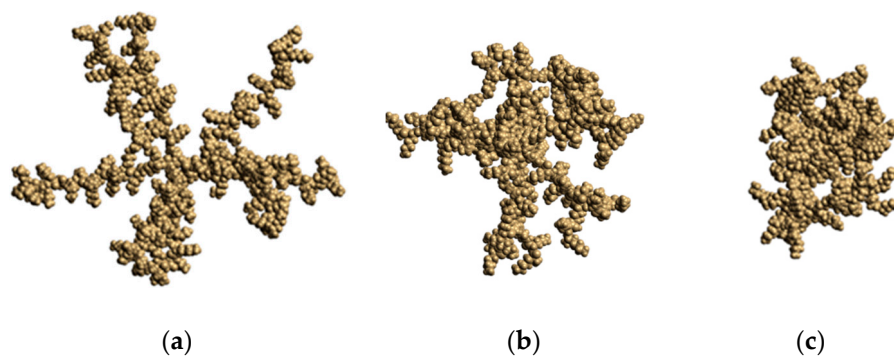


Figure 4. Snapshots of dendrigrafts: dendrigraft 1 (a); dendrigraft 2 (b); and dendrigraft 3 (c).

3.2. Internal Structure

The dendrigraft internal structure can be characterized by the density profiles of atoms $\rho(r)$ as:

$$\rho(r) = \frac{1}{4\pi r^2} \sum_i^{N_a} m_i \delta(r - r_{\text{com}}) \quad (3)$$

where N_a is the number of atoms, m_i is the mass of i -th atom, and r_{com} is the position of the dendrigraft's center of mass. The density profiles of the dendrigrafts are presented in Figure 5. It is easy to see that the density profiles of dendrigraft 1 and dendrigraft 2 are monotonous functions of distance r from the dendrigraft's center of mass. Thus, the profiles for dendrigraft 1 and dendrigraft 2 correspond to the dense-core and loose-shell model of dendrimers. It was shown earlier that this model was valid, for example, for such dendrimers as PAMAM and polysiloxane dendrimers [33–37].

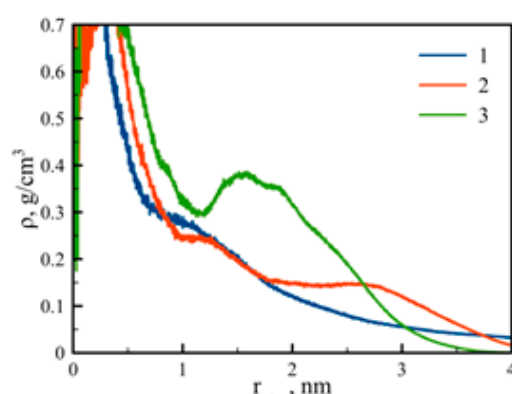


Figure 5. Normalized density profiles for dendrigrafts 1, 2, and 3 of generations $G = 3$, where r is the radial distance from the dendrigraft's center of mass.

However, in the case of dendrigraft 3, there is a minimum of density profile (cavity) at a distance near 1 nm from its center of mass similar to that obtained for non-regular dendrigrafts in [18]. It was shown earlier that the presence of the cavity could be due to the segregation effect between the dendrimer segments [38–40]. In the case of dendrigraft 3, this segregation can occur between internal non-charged and terminal charged monomers. This hypothesis is confirmed by the shape of distribution function of charged groups in dendrigraft 3 (Figure 6). It is easy to see that in the region of minimum density, there is also a minimum in charge density. It is obvious that uncharged monomers are less hydrophilic than charged ones. Therefore, we assume that the cavity (a low-density hydrophobic region) in dendrigraft 3 could be used for the encapsulation of hydrophobic drugs and other hydrophobic molecules for their delivery to target cells or organs.

For dendrigrafts 1 and 2, the charged groups are distributed along the contours of the side chains. Because of this reason (and the larger contour length of the side chains), their radial distribution is wide enough (see lines 1 and 2 in Figure 6a). Figure 6b demonstrates the distribution of the terminal charged groups. Line 1 (blue), for dendrigraft 1, shows the distribution of only eight groups, which are the ends of each of the eight linear side chains. With the increasing branching degree from dendrimer 1 to dendrimer 2, the peak moves towards the center of the dendrimer and becomes higher due to a decrease of contour length and an increase of terminal groups in each side chain, from 8 to 32. Dendrigraft 3 in Figure 6b demonstrates even more pronounced behavior because the contour length decreases and the number of terminal groups increases from 32 to 128. There is also a noticeable back-folding effect because the terminal groups fold and penetrate toward the central region of the dendrigrafts.

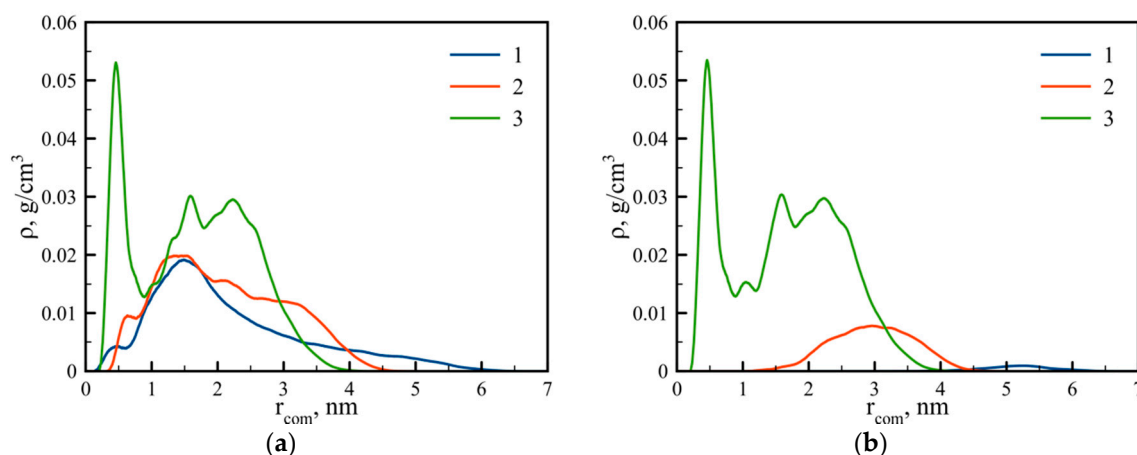


Figure 6. Distribution of (a) all charged NH_3^+ groups and (b) terminal charged NH_3^+ groups for dendrigrafts 1, 2, 3.

At the end we would like to check the distributions of end-to-end distances for the main chain (core region) of all dendrigrafts to understand if the main chain exists mainly in a coiled or in a stretched state. This distribution function is shown in Figure 7. It is easy to see that the distributions for all dendrigrafts are much wider than the corresponding distributions for end-to-end distances of side chains (see Figure 3). Thus the fluctuation of end-to-end distances is very large and the main chain is not always in the same state but passes through many possible states during simulation run.

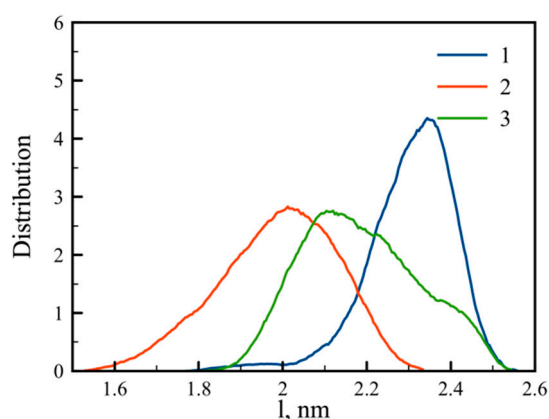


Figure 7. Distribution of end-to-end distance for dendrigrafts 1, 2, 3.

In addition, note that the distribution for dendrigraft 3 (line 3) in Figure 7 is between the distributions for dendrigrafts 1 and 2. This means that the stretching of the main chain of the dendrigraft is not a monotonous function of the number of branching points in the side chain (or contour length of the side chain). The reason for this is not quite clear and we plan to discuss it in more detail in a future paper.

4. Discussion

Three third-generation PLL dendrigrafts with the same molecular weight and number of charged groups, but with different topology (0, 3 and 7 branching points in each side chain) were simulated in water by a full-atomic MD method. This method has been used in the past for simulation of lysine dendrimers [14,20–23,41] and lysine dendrigrafts [18,24,25]. In addition to Gromacs software, we used approaches and computer programs elaborated earlier in [42–54]. We have shown in the

present paper that the size of dendrigraft depends on the branching point number. The higher the degree of branching, the smaller is the size of the dendrigraft. We found that sizes calculated from the simulations of dendrigrafts 2 and 3 (with three and seven branching points in each side chain, respectively) are in good agreement with the existing experimental data for PLL dendrigrafts [28,29]. At the same time, the size of dendrigraft 1 (with linear side chains) is essentially greater than that of experimental ones and it is likely that this topology is not realized in real lysine dendrigrafts.

We have shown that the radial density profile of a dendrigraft also depends on topology. In particular, for dendrigraft 1 and dendrigraft 2, the density profile is a monotonous function of the distance from the dendrigraft center of mass. For dendrigraft 3 (with a maximum number of branching points), there is a minimum of density profile at distances close to 1 nm from the dendrigraft's center of mass. There is also a minimum of charge distribution at this distance. This means that, at these distances, there is a cavity (a low density hydrophobic area inside the dendrigraft). We think that this feature could be important for using this particular dendrigraft as a nanocontainer for hydrophobic drugs.

We observed a wide distribution of end-to-end distance of the main chain (linear core) for all dendrigrafts. This means that core fluctuations are large and a dendrigraft could change its shape significantly. We also found that the end-to-end distance of the main chain of dendrigraft core has non-monotonous dependence on the topology (branching point number). The reason for this behavior is not clear but will be studied in more detail in a future paper in which more types of dendrigrafts with different branching point numbers will be studied.

Author Contributions: Contributions to Conceptualization, D.M. and I.N.; Methodology, D.M. and I.N.; Software, B.O. and M.I.; Validation, B.O., M.I., I.N., and D.M.; Formal Analysis, B.O. and M.I.; Investigation, B.O. and M.I.; Resources, D.M. and I.N.; Data Curation, B.O. and M.I.; Writing—Original Draft Preparation, B.O. and M.I.; Writing—Review and Editing, B.O., M.I., D.M., and I.N.; Visualization, B.O. and M.I.; Supervision, D.M. and I.N.; Project Administration, D.M., I.N.; Funding Acquisition, I.N.

Funding: Igor Neelov was financially supported by the Government of the Russian Federation (Grant 08-08).

Acknowledgments: The simulations have been performed by using Lomonosov supercomputers of Supercomputer Centre of Moscow State University and the Computer Resources Centre of Saint-Petersburg State University.

Conflicts of Interest: The authors declare no conflict of interest.

References

1. Bosman, A.W.; Janssen, H.M.; Meijer, E.W. About Dendrimers: Structure, Physical Properties, and Applications. *Chem. Rev.* **1999**, *99*, 1665–1688. [[CrossRef](#)] [[PubMed](#)]
2. Dykes, G.M. Dendrimers: A review of their appeal and applications. *J. Chem. Technol. Biotechnol.* **2001**, *76*, 903–918. [[CrossRef](#)]
3. Gittins, P.J.; Twyman, L.J. Dendrimers and supramolecular chemistry. *Supramol. Chem.* **2002**, *99*, 4782–4787. [[CrossRef](#)]
4. Gajbhiye, V.; Palanirajan, V.K.; Tekade, R.K.; Jain, N.K. Dendrimers as therapeutic agents: a systematic review. *J. Pharm. Pharmacol.* **2009**, *61*, 989–1003. [[CrossRef](#)] [[PubMed](#)]
5. Zimmerman, S.C.; Zeng, F.; Reichert, D.E.C.; Kolotuchin, S.V. Self-assembling dendrimers. *Science* **1996**, *271*, 1095–1098. [[CrossRef](#)] [[PubMed](#)]
6. Grayson, S.M.; Fréchet, J.M.J. Convergent dendrons and dendrimers: From synthesis to applications. *Chem. Rev.* **2001**, *101*, 3819–3868. [[CrossRef](#)] [[PubMed](#)]
7. Crespo, L.; Sanclimens, G.; Pons, M.; Giral, E.; Royo, M.; Albericio, F. Peptide and amide bond-containing dendrimers. *Chem. Rev.* **2005**, *105*, 1663–1681. [[CrossRef](#)] [[PubMed](#)]
8. Rao, C.; Tam, J.P. Synthesis of Peptide Dendrimer. *J. Am. Chem. Soc.* **1994**, *116*, 6975–6976. [[CrossRef](#)]
9. Darbre, T.; Reymond, J.L. Peptide dendrimers as artificial enzymes, receptors, and drug-delivery agents. *Acc. Chem. Res.* **2006**, *39*, 925–934. [[CrossRef](#)] [[PubMed](#)]

10. Klajnert, B.; Janiszewska, J.; Urbanczyk-Lipkowska, Z.; Bryszewska, M.; Shcharbin, D.; Labieniec, M. Biological properties of low molecular mass peptide dendrimers. *Int. J. Pharm.* **2006**, *309*, 208–217. [[CrossRef](#)] [[PubMed](#)]
11. Yao, H.; Veine, D.M.; Fay, K.S.; Staszewski, E.D.; Zeng, Z.Z.; Livant, D.L. The PHSCN dendrimer as a more potent inhibitor of human breast cancer cell invasion, extravasation, and lung colony formation. *Breast Cancer Res. Treat.* **2011**, *125*, 363–375. [[CrossRef](#)] [[PubMed](#)]
12. Tyssen, D.; Henderson, S.A.; Johnson, A.; Sterjovski, J.; Moore, K.; La, J.; Zanin, M.; Sonza, S.; Karellas, P.; Giannis, M.P.; et al. Structure activity relationship of dendrimer microbicides with dual action antiviral activity. *PLoS ONE* **2010**, *5*, e12309. [[CrossRef](#)] [[PubMed](#)]
13. Boyd, B.J.; Kaminskas, L.M.; Karellas, P.; Krippner, G.; Lessene, R.; Porter, C.J.H. Cationic poly-L-lysine dendrimers: Pharmacokinetics, biodistribution and evidence for metabolism and bioresorption after intravenous administration to rats. *Mol. Pharm.* **2006**, *3*, 614–627. [[CrossRef](#)] [[PubMed](#)]
14. Neelov, I.M.; Janaszewska, A.; Klajnert, B.; Bryszewska, M.; Makova, N.Z.; Hicks, D.; Pearson, H.; Vlasov, G.P.; Ilyash, M.Y.; Vasilev, D.S.; et al. Molecular properties of lysine dendrimers and their interactions with A β -peptides and neuronal cells. *Curr. Med. Chem.* **2013**, *20*, 134–143. [[CrossRef](#)] [[PubMed](#)]
15. Kodama, Y.; Nakamura, T.; Kurosaki, T.; Egashira, K.; Mine, T.; Nakagawa, H.; Muro, T.; Kitahara, T.; Higuchi, N.; Sasaki, H. Biodegradable nanoparticles composed of dendrigraft poly-L-lysine for gene delivery. *Eur. J. Pharm. Biopharm.* **2014**, *87*, 472–479. [[CrossRef](#)] [[PubMed](#)]
16. Tang, M.; Dong, H.; Li, Y.; Ren, T. Harnessing the PEG-cleavable strategy to balance cytotoxicity, intracellular release and the therapeutic effect of dendrigraft poly-L-lysine for cancer gene therapy. *J. Mater. Chem. B* **2016**, *4*, 1284–1295. [[CrossRef](#)]
17. Romestand, B.; Rolland, J.; Commeyras, A.; Desvignes, I.; Pascal, R.; Vandenabeele-trambouze, O. Dendrigraft Poly-L-lysine: A Non-Immunogenic Synthetic Carrier for Antibody Production. *Biomacromolecules* **2010**, *11*, 1169–1173. [[CrossRef](#)] [[PubMed](#)]
18. Francoia, J.-P.; Rossi, J.-C.; Monard, G.; Vial, L. Digitizing poly-L-lysine dendrigrafts: from experimental data to molecular dynamics simulations. *J. Chem. Inf. Model.* **2017**, *57*, 2173–2180. [[CrossRef](#)] [[PubMed](#)]
19. Roberts, B.P.; Scanlon, M.J.; Krippner, G.Y.; Chalmers, D.K. Molecular dynamics of poly(L-lysine) dendrimers with naphthalene disulfonate caps. *Macromolecules* **2009**, *42*, 2775–2783. [[CrossRef](#)]
20. Markelov, D.A.; Falkovich, S.G.; Neelov, I.M.; Ilyash, M.Y.; Matveev, V.; Lahderanta, E.; Ingman, P.; Darinskii, A. Molecular dynamics simulation of spin-lattice NMR relaxation in poly-L-Lysine dendrimers: Manifestation of the semiflexibility effect. *Phys. Chem. Chem. Phys.* **2015**, *17*, 3214–3226. [[CrossRef](#)] [[PubMed](#)]
21. Falkovich, S.; Markelov, D.; Neelov, I.; Darinskii, A. Are structural properties of dendrimers sensitive to the symmetry of branching? Computer simulation of lysine dendrimers. *J. Chem. Phys.* **2013**, *139*, 064903. [[CrossRef](#)] [[PubMed](#)]
22. Neelov, I.; Markelov, D.; Falkovich, S.; Ilyash, M.; Okrugin, B.; Darinskii, A. Mathematical modeling of lysine dendrimers temperature dependencies. *Polym. Sci. Ser. C* **2013**, *55*, 154–161. [[CrossRef](#)]
23. Neelov, I.; Ilyash, M.; Falkovich, S.; Darinskii, A. Computer simulation of lysine dendrimers by molecular dynamics method. *Smart Nanocompos.* **2014**, *5*, 127.
24. Neelov, I.M.; Okrugin, B.M.; Falkovich, S.G.; Darinskii, A.A. Computer simulation of new type of branched peptides-lysine dendrigrafts. In Proceedings of the 8th International Symposium: Molecular Order and Mobility in Polymers, St. Petersburg, Russia, 2–6 June 2014; Abstract Number O-13. p. 31.
25. Neelov, I.; Popova, E. Interaction of Lysine Dendrigraft of 2nd Generation and Semax Peptide. Molecular Dynamics Simulation. In Proceedings of the International Conference on Control, Artificial Intelligence, Robotics & Optimization (ICCAIRO), Prague, Czech Republic, 20–22 May 2017; pp. 182–186.
26. Hess, B.; Kutzner, C.; Van Der Spoel, D.; Lindahl, E. GROMACS 4: Algorithms for highly efficient, load-balanced, and scalable molecular simulation. *J. Chem. Theor. Comput.* **2008**, *4*, 435–447. [[CrossRef](#)] [[PubMed](#)]
27. Berendsen, H.J.C.; Postma, J.P.M.; Gunsteren, W.F.; Dinola, A.; Haak, J.R. Molecular dynamics with coupling to an external bath. *J. Chem. Phys.* **1984**, *81*, 3684–3690. [[CrossRef](#)]
28. Cottet, H.; Martin, M.; Papillaud, A.; Souaid, E.; Collet, H.; Commeyras, A. Determination of dendrigraft poly-L-lysine diffusion coefficients by Taylor dispersion analysis. *Biomacromolecules* **2007**, *8*, 3235–3243. [[CrossRef](#)] [[PubMed](#)]

29. Yevlampieva, N.; Dobrodumov, A.; Nazarova, O.; Okatova, O.; Cottet, H. Hydrodynamic behavior of dendrigraft polylysines in water and dimethylformamide. *Polymers* **2012**, *4*, 20–31. [[CrossRef](#)]
30. Baigude, H.; Katsuraya, K.; Okuyama, K.; Tokunaga, S.; Uryu, T. Synthesis of sphere-type monodispersed oligosaccharide-polypeptide dendrimers. *Macromolecules* **2003**, *36*, 7100–7106. [[CrossRef](#)]
31. Lederer, A.; Hartmann, T.; Komber, H. Sphere-like fourth generation pseudo-dendrimers with a hyperbranched core. *Macromol. Rapid Commun.* **2012**, *33*, 1440–1444. [[CrossRef](#)] [[PubMed](#)]
32. Maiti, P.K.; Cagin, T.; Wang, G.; Goddard, W.A. Structure of PAMAM dendrimers: Generations 1 through 11. *Macromolecules* **2004**, *37*, 6236–6254. [[CrossRef](#)]
33. Götze, I.O.; Likos, C.N. Conformations of flexible dendrimers: A simulation study. *Macromolecules* **2003**, *36*, 8189–8197. [[CrossRef](#)]
34. Kłos, J.S.; Sommer, J.-U. Properties of dendrimers with flexible spacer-chains: A Monte Carlo study. *Macromolecules* **2009**, *42*, 4878–4886. [[CrossRef](#)]
35. González, M.A.; Abascal, J.L.F. The shear viscosity of rigid water models. *J. Chem. Phys.* **2010**, *132*, 096101. [[CrossRef](#)] [[PubMed](#)]
36. Venable, R.M.; Hatcher, E.; Guvench, O.; MacKerell, A.D.; Pastor, R.W. Comparing simulated and experimental translation and rotation constants: Range of validity for viscosity scaling. *J. Phys. Chem. B* **2010**, *114*, 12501–12507. [[CrossRef](#)] [[PubMed](#)]
37. Timoshenko, E.G.; Kuznetsov, Y.A.; Connolly, R. Conformations of dendrimers in dilute solution. *J. Chem. Phys.* **2002**, *117*, 9050. [[CrossRef](#)]
38. Markelov, D.A.; Matveev, V.V.; Ingman, P.; Nikolaeva, M.N.; Lähderanta, E.; Shevelev, V.A.; Boiko, N.I. NMR studies of carbosilanedendrimer with terminal mesogenic groups. *J. Phys. Chem. B* **2010**, *114*, 4159–4165. [[CrossRef](#)] [[PubMed](#)]
39. Markelov, D.A.; Mazo, M.A.; Balabaev, N.K.; Gotlib, Y.Y. Temperature dependence of the structure of a carbosilanedendrimer with terminal cyanobiphenyl groups: Molecular-dynamics simulation. *Polym. Sci. Ser. A* **2013**, *55*, 53–60. [[CrossRef](#)]
40. Markelov, D.A.; Polotsky, A.A.; Birshstein, T.M. Formation of a “Hollow” interior in the fourth-generation dendrimer with attached oligomeric terminal segments. *J. Phys. Chem. B* **2014**, *118*, 14961–14971. [[CrossRef](#)] [[PubMed](#)]
41. Neelov, I.; Falkovich, S.; Markelov, D.; Paci, E.; Darinskii, A.; Tenhu, H. Molecular dynamics of lysine dendrimers: Computer simulation and NMR. In *Dendrimers in Biomedical Applications*; Klajnert, B., Ed.; Royal Society of Chemistry: London, UK, 2013; pp. 99–114. [[CrossRef](#)]
42. Neelov, I.; Adolf, D. Brownian dynamics simulations of dendrimers under elongational flow: Bead-rod model with hydro-dynamic interactions. *Macromolecules* **2003**, *36*, 6914–6924. [[CrossRef](#)]
43. Ennari, J.; Elomaa, M.; Neelov, I. Modeling of water-free and water containing solid polyelectrolytes. *Polymer* **2000**, *41*, 985–990. [[CrossRef](#)]
44. Neelov, I.M.; Binder, K. Brownian dynamics of grafted polymer chains-time-dependent properties. *Macromol. Theor. Simul.* **1995**, *4*, 1063–1084. [[CrossRef](#)]
45. Darinskii, A.; Gotlib, Y.; Lyulin, A.; Neelov, I. Computer simulation of local dynamics of a polymer chain in the orienting field of the liquid crystal type. *Polym. Sci. USSR* **1991**, *33*, 1116–1125. [[CrossRef](#)]
46. Darinsky, A.; Lyulin, A.; Neelov, I. Computer simulations of molecular motion in liquid crystals by the method of brownian dynamics. *Macromol. Chem. Theory Simul.* **1993**, *2*, 523–530. [[CrossRef](#)]
47. Ennari, J.; Neelov, I.; Sundholm, F. Simulation of a PEO based solid polyelectrolyte, comparison of the CMM and the Ewald summation method. *Polymer* **2000**, *41*, 2149–2155. [[CrossRef](#)]
48. Mazo, M.A.; Shamaev, M.Y.; Balabaev, N.K.; Darinskii, A.A. Conformational mobility of carbosilanedendrimer: Molecular dynamics simulation. *Phys. Chem. Chem. Phys.* **2004**, *6*, 1285–1289. [[CrossRef](#)]
49. Neelov, I.M.; Adolf, D.B.; McLeish, T.C.; Paci, E. Molecular dynamics simulation of dextran extension by constant force in single molecule AFM. *Biophys. J.* **2006**, *91*, 3579–3588. [[CrossRef](#)] [[PubMed](#)]
50. Shavykin, O.V.; Neelov, I.M.; Darinskii, A.A. Is the manifestation of the local dynamics in the spin-lattice NMR relaxation in dendrimers sensitive to excluded volume interactions? *Phys. Chem. Chem. Phys.* **2016**, *18*, 24307–24317. [[CrossRef](#)] [[PubMed](#)]

51. Shavykin, O.V.; Mikhailov, I.V.; Neelov, I.M.; Darinskii, A.A.; Leermakers, F.A.M. Effect of an asymmetry of branching on structural characteristics of dendrimers revealed by Brownian dynamics simulations. *Polymer* **2018**, *146*, 256–266. [[CrossRef](#)]
52. Ennari, J.; Neelov, I.; Sundholm, F. Molecular dynamics simulation of the structure of PEO based solid polymer electrolytes. *Polymer* **2000**, *41*, 4057–4063. [[CrossRef](#)]
53. Neelov, I.M.; Adolf, D.B. Brownian dynamics simulation of hyperbranched polymers under elongational flow. *J. Phys. Chem. B* **2004**, *108*, 7627–7636. [[CrossRef](#)]
54. Ennari, J.; Neelov, I.; Sundholm, F. Estimation of the ion conductivity of a PEO-based polyelectrolyte system by molecular modeling. *Polymer* **2001**, *42*, 8043–8050. [[CrossRef](#)]



© 2018 by the authors. Licensee MDPI, Basel, Switzerland. This article is an open access article distributed under the terms and conditions of the Creative Commons Attribution (CC BY) license (<http://creativecommons.org/licenses/by/4.0/>).